Flow distribution on the shellside of a cylindrical shell and tube heat exchanger

T. Pekdemir and T. W. Davies
School of Engineering, University of Exeter, Exeter, UK

L. E. Haseler and A. D. Diaper
AEA Technology Harwell, Oxfordshire, UK

Shellside cross-flow velocity distributions and pressure drops within the tube bundle of an E-type segmented baffle model cylindrical shell and tube heat exchanger have been measured using a neutral-density particle-tracking technique and pressure tapped instrument tubes respectively. Shellside flow Reynolds numbers were varied in the range 301–2177. The measurements were confined to one interbaffle space (the fifth downstream of an eight baffle tube bundle). Only one baffle cut was employed (25 percent). In the context of multistream modeling of the shellside flow, the experiments were designed to shed light on the magnitude of and variation in the cross-flow component of the shellside flow within the tube bundle. Comparison of the measured pressure-drop distributions, interpreted as corresponding cross-flow velocity distributions, with direct cross-flow velocity measurements lends credibility to the application of pressure-drop correlations for flow across tube bundles and further clarifies the nature of shellside flow. A collateral objective was to investigate the relationship between the characteristics of cross-flow within the bundle and the more readily observable cross-flow behavior in the bypass region. In addition, the results were used to test an empirical method of predicting overall cross-flow fractions in tube bundles. The results show a marked heterogeneity of the cross-flow in the plane of velocity measurements (a central, horizontal pass partition lane) and provide pointers for the refinement of computer models of shellside flow behavior.

Keywords: shellside flows; flow in tube bundles; cross-flow velocities; cross-flow fractions

Introduction

Crudely designed shell and tube heat exchangers often have higher capital and operating costs than more accurate designs. One area where there is room for improvement in design procedures is the way in which shellside flow is modeled. Shellside flow is a complex three-dimensional (3-D) process and is influenced by such things as manufacturing clearances and tolerances, expansions and contractions in flow area, flow obstructions, baffles, and sealing strips. The flow distribution is often conveniently represented by a number of one-dimensional (1-D) flows known as flow streams, i.e., cross-flow, cross-flow bypass, window flow, shell-baffle and tube-baffle leakage flows, and pass partition flow.

Comparatively few measurements of shellside flow distributions have been reported in the open literature. Diaper and Haseler (1990) measured the velocity distribution in the bypass lane in the model shell and tube heat exchanger used in the present work, using the same experimental technique as employed by the present authors. They determined bypass flow fractions from their velocity measurements in the bypass flow region. Gupta and Katz (1957) visualized the shellside flow by introducing tracer particles, using a small glass cylindrical exchanger. Their rig had only 26 tubes in a 152.4-mm shell, which is far from being representative of commercial designs. Berner et al. (1984) studied flow around baffles within a tubeless plexiglass rectangular shell of cross section 30 cm × 6 cm. The flow was visualized by dye injection and aluminium tracer particles. Perez (1984) obtained a comprehensive shellside flow visualization in a 101.6-mm cylindrical shell containing 92 6.35-mm tubes using an oil-lampblack technique. The work reported here forms part of a series of increasingly detailed studies of shellside flow, the first of which was conducted by Murray (1988) for HTFS, the Heat Transfer and Fluid Flow Service at the Harwell Laboratory; his apparatus was essentially that used in the present work, and he used a dye injection technique to visualize the flow across the tube bundle.

In the design of shell and tube heat exchangers, the magnitude of the pressure drop is generally of great importance. Although shellside pressure drop has been extensively investigated and reported in the open literature and many prediction methods have been constructed for modeling the shellside flow, most of this work has been carried out on laboratory-size equipment or equipment lacking realism in some respects. Previous work in this area included that of Brown (1956), who studied pressure drop in a cylindrical baffled shell and tube E-type heat exchanger consisting of 80 tubes of 0.95-cm outer diameter in a staggered square arrangement with a diagonal pitch to a

Address reprint requests to Professor Davies at the School of Engineering, University of Exeter, Engineering Building, North Park Road, Exeter EX4 4QP, UK.

Received 21 November 1991; accepted 13 April 1992

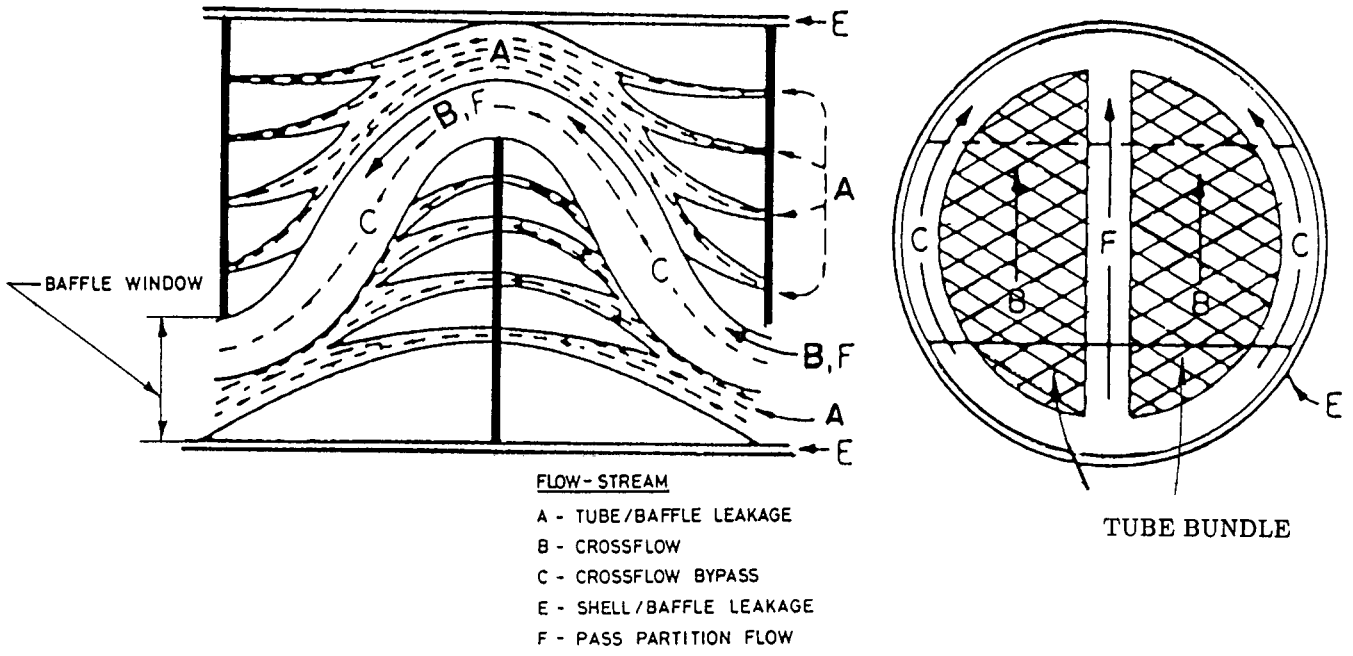

Figure 1 Idealized diagram of shellside flow streams (adapted from Tinker (1947) and Palen and Taborek (1969) after Bell (1980))

diameter ratio of 3.18 in a 13.34-cm internal diameter shell. Leighton (1955) measured pressure drops in a larger cylindrical exchanger consisting of 470 tubes of 0.64-cm diameter on an equilateral triangular arrangement with a diagonal pitch to a diameter ratio of 3.38 in a 21.27-cm outer diameter shell. Both studies were parts of the Delaware University Research Program using rigs known as Model 9 and Model 10, respectively. This program ran from 1947 to 1963 and has made a remarkable contribution to the understanding of shellside flow. This so-called "Delaware Project" provided an extensive amount of data for the development of design methods and models such as those currently used by HTFS, which have been employed during the course of the present study. Zukauskas et al. (1983) obtained a large amount of pressure-drop data for the flow of gases across tube bundles. The results and correlations produced from such work are summarized in the Heat Exchangers Design Handbook (Zukauskas and Ulinskas 1983) along with a selection of data from the literature. Murray (1988) obtained a large amount of pressure-drop measurements using the same experimental apparatus and technique as used in the present work. He compared his experimental measurements with previously obtained data such as those of Leighton (1955). He reported a low velocity separated and recirculating zone just downstream of each baffle tip, this being larger near the shell wall than at the shell central plane. He also reported that cross-flow velocities in the baffle overlap region were not uniform across the baffle space.

Some assumed relationship between shellside pressure drop and shellside flow distribution is often used to model, analyze, and predict shellside flow patterns. Two general design methods are well known: the single-stream method and the multistream method. The concept of a multistream model was first introduced by Tinker (1947) and later adapted by some other authors such as Palen and Taborek (1969), Bell (1980), and Johnston and Wills (1984). It is based on a set of flows as shown in Figure 1.

Various methods can be chosen for modeling each of the component flows, and there are still uncertainties about the component flow correlations. The correlations for the shellside flow, in particular the cross-flow and bypass components, have often been generated on small-scale experimental apparatus having a significantly different geometry from that found in

Notation

A_c Cross-flow area of tube-free duct (m^2)
A_{ct} Average cross-flow area available for flow including bypass gap (m^2)
C Pressure-drop loss coefficient
d_{min} Minimum gap between the tubes (m)
D_t Tube diameter (m)
L Length of the cross-flow section (m)
M_c Cross-flow mass flow rate (kg/m^2)
Re Reynolds number $= \dfrac{M_c d_{min}}{\mu A_{ct}}$
Re_c Cross-flow Reynolds number $= \dfrac{M_c D_t}{\mu A_c}$
Re_{mg} Minimum gap Reynolds number $= \dfrac{U_{max} d_{min} \rho}{\mu}$
U_{max} Cross-flow velocity in the minimum gap between the tubes (m/s)
V_c Cross-flow velocity (m/s)
ΔP_c Cross-flow pressure drop (N/m^2)

Greek symbols

ρ Density of the shellside fluid (kg/m^3)
μ Viscosity of the shellside fluid ($N \cdot s/m^2$)
φ_1 Viscosity correction factor
φ_2 Roughness correction factor

practical exchangers. In the past, in view of this uncertainty, designers often used a simple single-stream model with a series of "correction factors" derived by correlating overall pressure drop for various shellside geometries. Such methods, however, have limited validity beyond the range of shellside geometries on which they are based. More realistic methods must be based on the better understanding provided by multistream models, and the present study provides data that may be used to refine such models.

Experimental apparatus

Isothermal experiments were carried out on the HTFS Shellside Flow Visualisation Rig. Using this facility, it is possible to model and control all the main features of a shell and tube heat exchanger and, since the rig is of an all-glass construction, flow visualization and optical probing of the shellside flow is also possible.

The exchanger model consists essentially of (1) a cylindrical glass shell, which contains (2) a removable stainless steel tube bundle framework, which supports (3) a bundle of (mainly) glass rods ("tubes") together with strategically placed instrument tubes, which were used to measure local pressure in the shellside flow, i.e., water. The important dimensions and features of the rig are given in Table 1. A full description of the rig has been given by Pekdemir (1990). Further work on this exchanger with different baffle cuts and spacings and different leakage configurations is in progress. Some preliminary findings have been reported by Keene et al. (1991).

A cross section of the bundle is shown in Figure 2a. The middle horizontal row of the bundle was removed in order to create a pass partition lane of 9.21-mm height. The pass partition lane within the test section was illuminated by using an optical system and a 5-watt Argon ion laser, as shown in Figures 2b and 2d, so that particle tracks could be followed in that lane. The illumination was applied selectively via the vacant tube holes in the baffles. These holes were covered with microscope slide glass in order to prevent flow but to allow the light to pass. The holes in the baffles away from the test compartment were sealed with neoprene gaskets, which also sealed the areas of leakage flows between the edges of the baffles and the shell walls and between the tubes and the tube holes in the baffles, simplifying the shellside flow pattern by eliminating leakage flows.

Table 1 Main dimensions and features of the shellside flow rig

Item	Dimensions and descriptions
Inside diameter of shell (mm)	300 ± 0.1
Diameter of tubes (mm)	12 ± 0.4
Length of tubes	1206 ± 0.1
Number of tubes	252
Tube arrangement	Rotated square
Diagonal pitch/tube diameter	1.25
Longitudinal pitch/tube diameter	0.88
Transverse pitch/tube diameter	1.77
Baffle type	Single segmental
Baffle cut	25% of shell inside diameter
Diameter of tube holes in baffles (mm)	12.4 ± 0.1
Number of baffles	8
Baffle spacing (mm)	110.4
Baffle thickness (mm)	4.59
Thickness of neoprene gaskets on baffles (mm)	1.59
Inlet and outlet nozzle inside diameter (mm)	80
Inlet end spacing (mm)	150
Outlet end spacing (mm)	250
Total length of baffled region (mm)	1158
Largest shell-bundle clearance (mm)	32.24
Smallest shell-bundle clearance (mm)	13.12

Isothermal conditions were maintained by means of a cooling coil, situated in the supply tank. Polystyrene beads of 0.5-mm diameter were used as neutrally buoyant flow-following particles. A high-speed video recording system, capable of 1,000 frames per second, was used for recording the particle tracks.

Pressure-tapped instrument tubes were used for the measurements of pressure distributions in the bundle of the model exchanger. The position of these pressure-sensing tubes in the tube bundle is shown in Figures 2a and 2b. There were ten such tubes in all. A schematic view of a pressure sensing tube is shown in Figure 3. These tubes protruded beyond each end of the shell, through O-ring seals in the end plates so that axial movement provided the means of measuring pressure distributions across the baffle space.

Experimental procedure

The cross-flow velocity within the horizontal pass partition lane in the bundle was measured for four different total shellside flowrates of 24, 12, 6, and 3 $m^3\,hr^{-1}$. These correspond to the "minimum gap" Reynolds numbers of 2,177, 1,104, 510, and 301, where Re is defined as

$$\mathrm{Re}_{mg} = \frac{U_{max} d_{min} \rho}{\mu} \tag{1}$$

where U_{max} is the maximum crossflow velocity, near the exchanger centerline, in the minimum gap between the tubes, d_{min} is the minimum gap between the tubes (see Figure 5), and ρ and μ are the density and the viscosity of the shellside fluid. Velocities were measured at six different radial positions in the tube bundle, as indicated in Figures 2a and 2d. The laser light was directed to the required region using four thin vertical mirrors set at 45° to the exchanger axis, two in each of the baffle compartments upstream and downstream of the one where the measurements were made, as illustrated in Figure 2d. The illuminated regions in which particles could be tracked corresponded with the positions from which the tubes had been removed to create the pass partition lane. Any of these six regions were selected by changing the position of the external mirrors directing the laser beam. With such side illumination, the particles appeared as bright spots against a dark background when viewed from the camera position. The video speed and recording time were selected according to the shellside flow rate as shown in Table 2. The field of view of the camera was set to record the full width (i.e., baffle-to-baffle) of the pass partition lane. The flow was downward in the baffle

Table 2 Video speed and recording time at each of Reynolds numbers studied

Reynolds number	Video speed (frame·s^{-1})	Recording time (s)
2177	1000	6
1104	1000	6
510	500	12
301	250	24

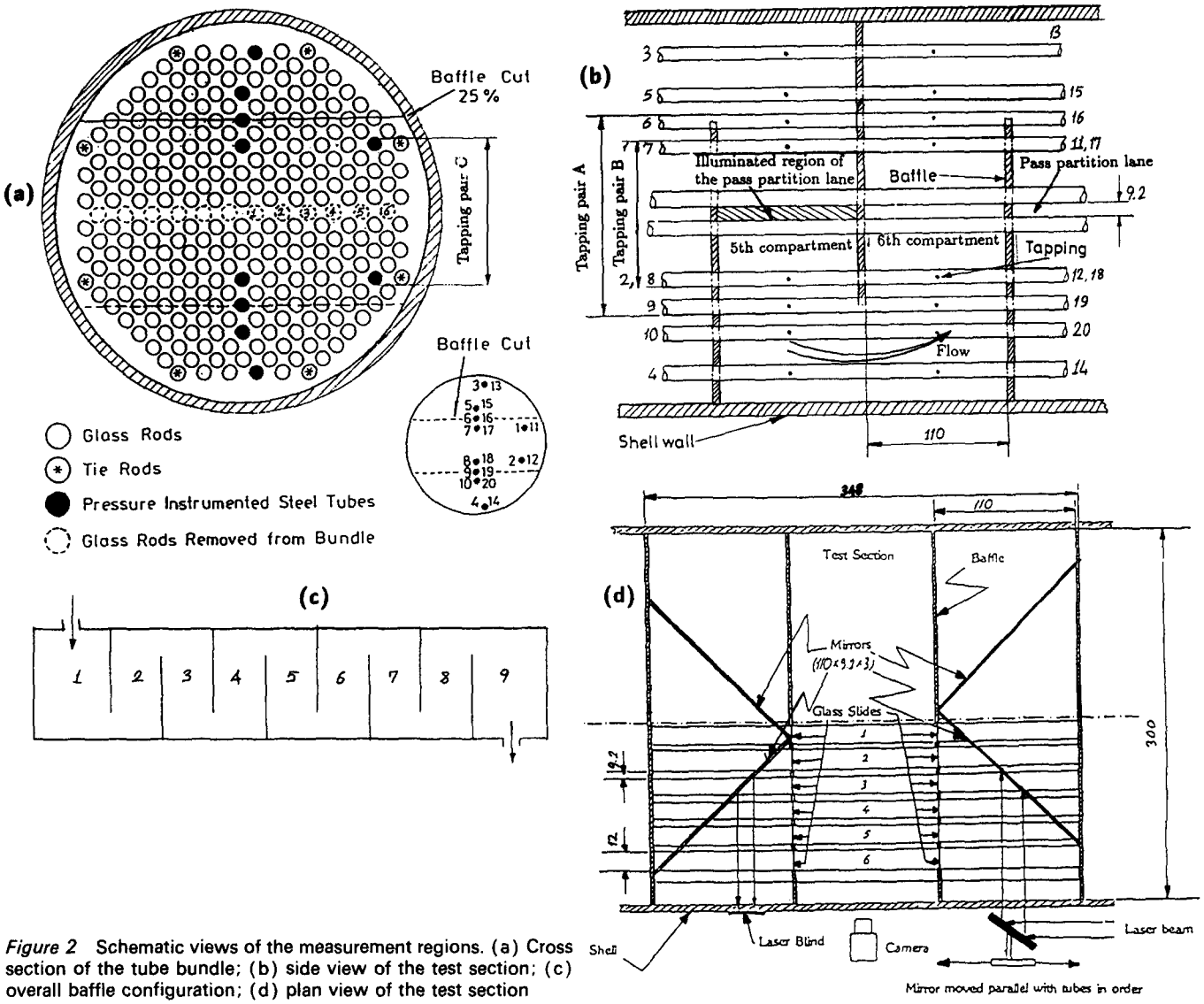

Figure 2 Schematic views of the measurement regions. (a) Cross section of the tube bundle; (b) side view of the test section; (c) overall baffle configuration; (d) plan view of the test section

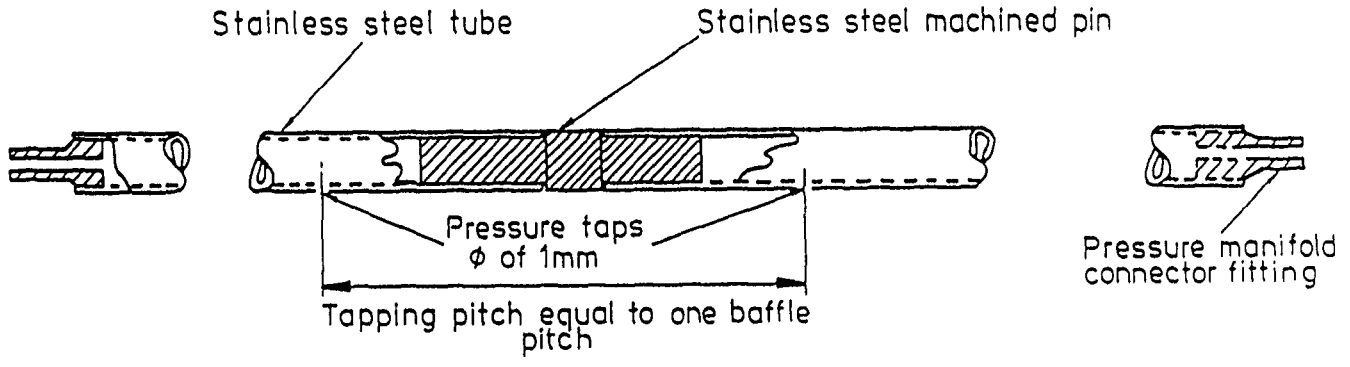

Figure 3 Pressure sensing tube

compartment studied. The average number of the particles present in a particular frame was approximately four.

Particle image recognition and measurement between frames was accomplished using a computer-based particle tracking technique developed at Harwell known as "Diamond" (as described by Diaper and Haseler 1990a).

The shellside flow pressure distribution was discretely sampled in strategic locations for Reynolds numbers in the range $270 < \mathrm{Re} < 2{,}200$, where

$$\mathrm{Re} = \frac{M_c d_{\min}}{\mu A_{ct}} \tag{2}$$

where M_c is the crossflow mass flowrate and A_{ct} is the average crossflow area available for flow including the bypass gap. All differential pressure measurements were recorded with reference to one tapping, number 13 (see Figures 2a and 2b), which remained in the same position throughout the experiments.

Interpretation of velocity data

The locations of the measurement regions used, shown in Figure 4, were dictated by the geometry of the tube bundle arrangement. Since the objective of the study was to obtain information on the distribution of cross-flow within the bundle, the relationship between the flow in the sampling positions and the general cross-flow was investigated. The illuminated regions where the particle tracks were recorded were circular in cross section, but the observable regions were actually slightly smaller than the diameter of the removed tubes because of the shading effect of the adjacent tube rows, as illustrated in Figure 4. Examination of Figure 4 suggests that with the given staggered tube positions, flow from the top half to the bottom half of the bundle across the pass partition lane will be mainly through the illuminated regions. In order to confirm this, detailed calculations were performed using the computational fluid dynamics code HARWELL-FLOW3D, to predict velocities in a horizontal pass partition lane in an infinite tube bundle. FLOW3D is a finite-difference code capable of solving flow equations in three dimensions for complex geometries. The calculation grid was that which had previously been used by Diaper and Haseler (1990b) to predict the pressure loss coefficient in an infinite bundle by calculating flows over five tube rows. The predicted velocity variation along the centerline of the tube-free transverse pass partition lane is shown in Figure 5 for a maximum gap velocity of 0.4 ms^{-1}. It can be seen that negative velocities are predicted midway between the illuminated regions, indicating a recirculation zone behind the last tube rows of the top half of the bundle. From this velocity profile it can be inferred that on the shell centerline the main cross-flow is confined to a region 5.6 mm on each side of the center of the missing tubes, since beyond the edges of this region the positive and negative velocities integrate to zero. This predicted effective cross-flow area is to be compared with the 6-mm radius of the illuminated measurement region. Above and below the centerline the illuminated region is narrower, while the main cross-flow area predicted by FLOW3D is rather wider, so that the average width of the predicted cross-flow is actually about 10 percent greater than that of the illuminated region. On this basis it was assumed that the measured mean velocities in the illuminated region together with the mean width of the illuminated region could be used to determine the shellside centerplane cross-flow to within an accuracy of about 10 percent.

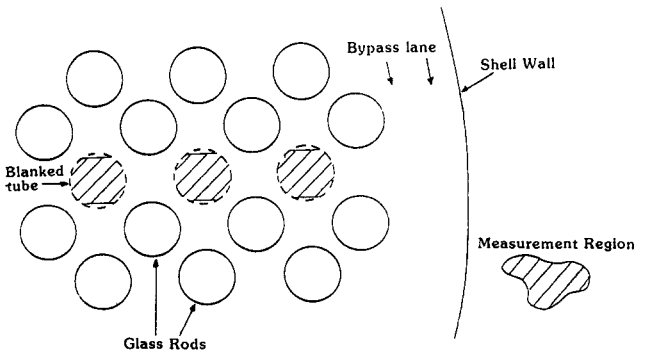

Figure 4 Regions where cross-flow measurements were made

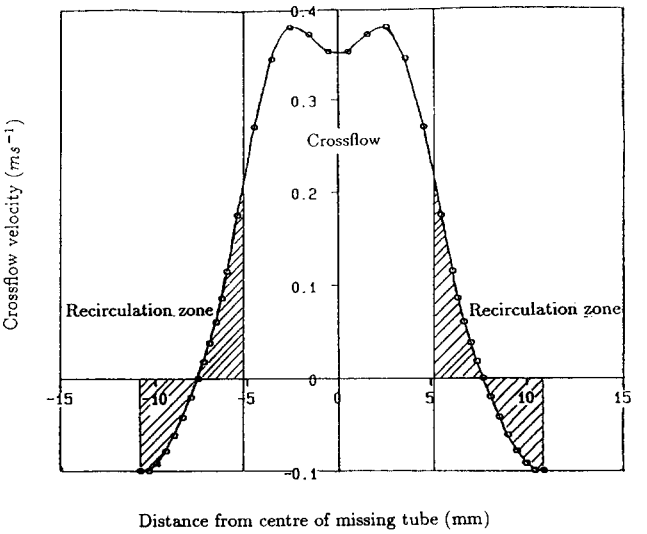

Figure 5 Predicted flow velocity across a tube space (−10.6 mm to +10.6 mm) in the pass partition lane

Flow rate estimation

Particle track data collected were arbitrarily scattered and widely distributed along the horizontal space between the upstream and downstream baffles and were presumed to be a representative sample taken from the type of flow field predicted by FLOW3D and shown in Figure 5. Data in this form gave qualitative information and showed the general tendencies of the radial and axial distributions of cross-flow in the pass partition lane. Figure 6 shows representative velocity distributions of this form for the minimum gap Reynolds number of 1,104 and for the six "tube positions" numbered radially outwards from the central plane of the bundle (see Figure 2). There were typically about 120 particle tracks recorded at each "tube position." These were, however, not always uniformly spread across the baffle space. To obtain representative velocities, each of the tube positions was divided into seven intervals along the axial distance between the upstream and downstream baffles that defined the measurement region. Average velocities in each interval were then used to construct a flow profile for each tube position and each flowrate being studied. The mean velocities in each interval were also averaged in order to find "tube mean velocity" for each of six tube positions. Then finally the overall cross-flow velocities were calculated by averaging these mean velocities for all the six tube positions.

In a few cases, as seen in Figure 6, some negative velocities were recorded, assumed to be due to the recirculation zones formed behind the last tube row immediately above the pass partition lane. Since the objective was to calculate cross-flow velocity, these recirculation zone data were filtered from the main data, and the remaining data were averaged by the method described above. The maximum difference between the velocities calculated from filtered and unfiltered data was ±6.86 percent. Regression analysis was applied to the original particle track data, and Figure 6 shows the best-fit curves where Y is the cross-flow velocity (ms^{-1}) and X is the distance between the baffles (m).

The data were further analyzed in order to obtain mass flow-rate distributions and the cross-flow fraction in the pass partition lane. Cross-flow mass flow rate, and therefore the cross-flow fraction for each interval, were calculated relative to the total flow through the exchanger, assumed to be distributed uniformly among all the intervals on all tube positions in the

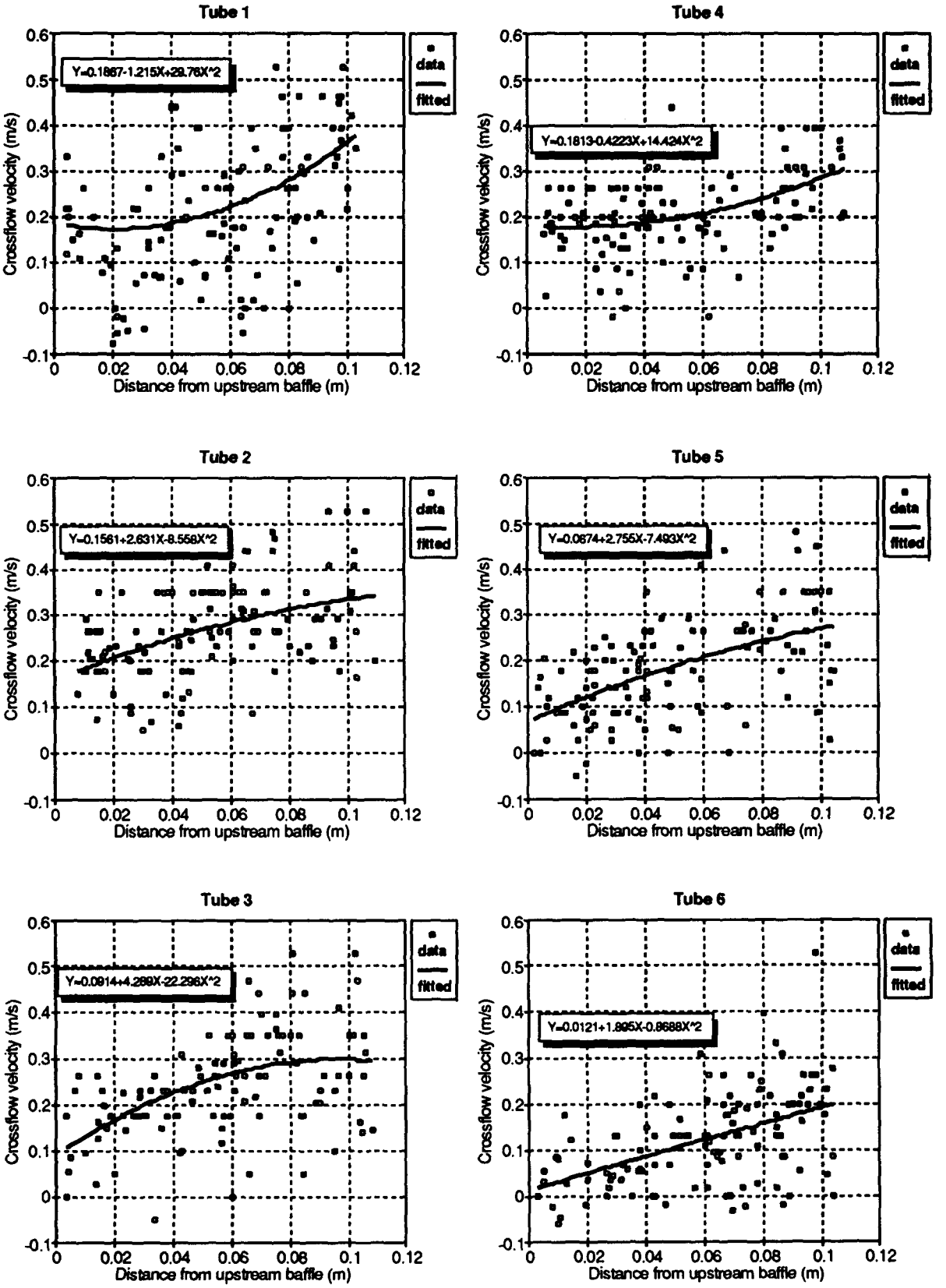

Figure 6 Measured cross-flow velocity distributions in a baffle compartment showing fitted profiles for the minimum gap Reynolds number (Re) = 1,104

Table 3 Comparison of overall cross-flow percentages derived from the present data, Diaper and Haseler's (1990a) data, and the predictions of the ESDU (1974, 1979) standard

1	2	3	4	5	6
2177	69.80	71.80	70.20	77.40	64.40
1104	69.60	72.60	70.40	71.90	62.60
510	69.50	74.60	68.70	68.20	60.40
301	74.90	79.80	61.20	67.60	59.30

Column 1: Shellside flow Reynolds numbers; column 2: Present work, calculated cross-flow percentages before filtering out recirculation zone data; column 3: Present work, calculated cross-flow percentages after filtering out recirculation zone data; column 4: Present work, calculated cross-flow percentages from pressure-drop measurements by using ESDU (1974, 1979) standard; column 5: Cross-flow percentages derived from velocity measurements in the bypass region (after Diaper and Haseler 1990a); column 6: ESDU (1974, 1979) predictions

pass partition lane. A density of 996 kg m^{-3} and a flow area of 0.0141 m^2 were used in the calculation of the cross-flow fractions. The total shellside cross-flow fractions calculated by the above technique are compared in Table 3 with those calculated by using the predictions of ESDU (1979), which may be used to estimate the cross-flow fraction in a given tube bundle geometry. Also included is Diaper and Haseler's (1990a) estimates, made using particle track data obtained previously in the bypass region of the same heat exchanger model. As seen from Table 3, cross-flow fractions, variously estimated, are generally in good agreement apart from a sudden rise in the fractions calculated from the present direct cross-flow velocity measurements in the horizontal pass partition lane at Reynolds number = 300. It should be remembered that the fractions calculated from direct cross-flow velocity measurements are local cross-flow fractions in the pass partition lane, whereas other observations and predictive results give the mean cross-flow fractions over the entire cross-flow region. It may be that at lower Reynolds number, bypassing is not so prevalent.

Cross-flow variation in the pass partition lane

Velocity variations in the chosen baffle compartment as a function of the distance between the upstream and the downstream baffles are shown in Figure 7 for four flow rates corresponding to minimum gap Reynolds numbers of 2177, 1104, 510, and 301, respectively. Features of the shellside flow observable from this figure may be summarized as follows:

- the cross-flow velocity in a baffle space is larger near the downstream baffle. This is to be expected because of the effects of flow separation at the upstream baffle edge and

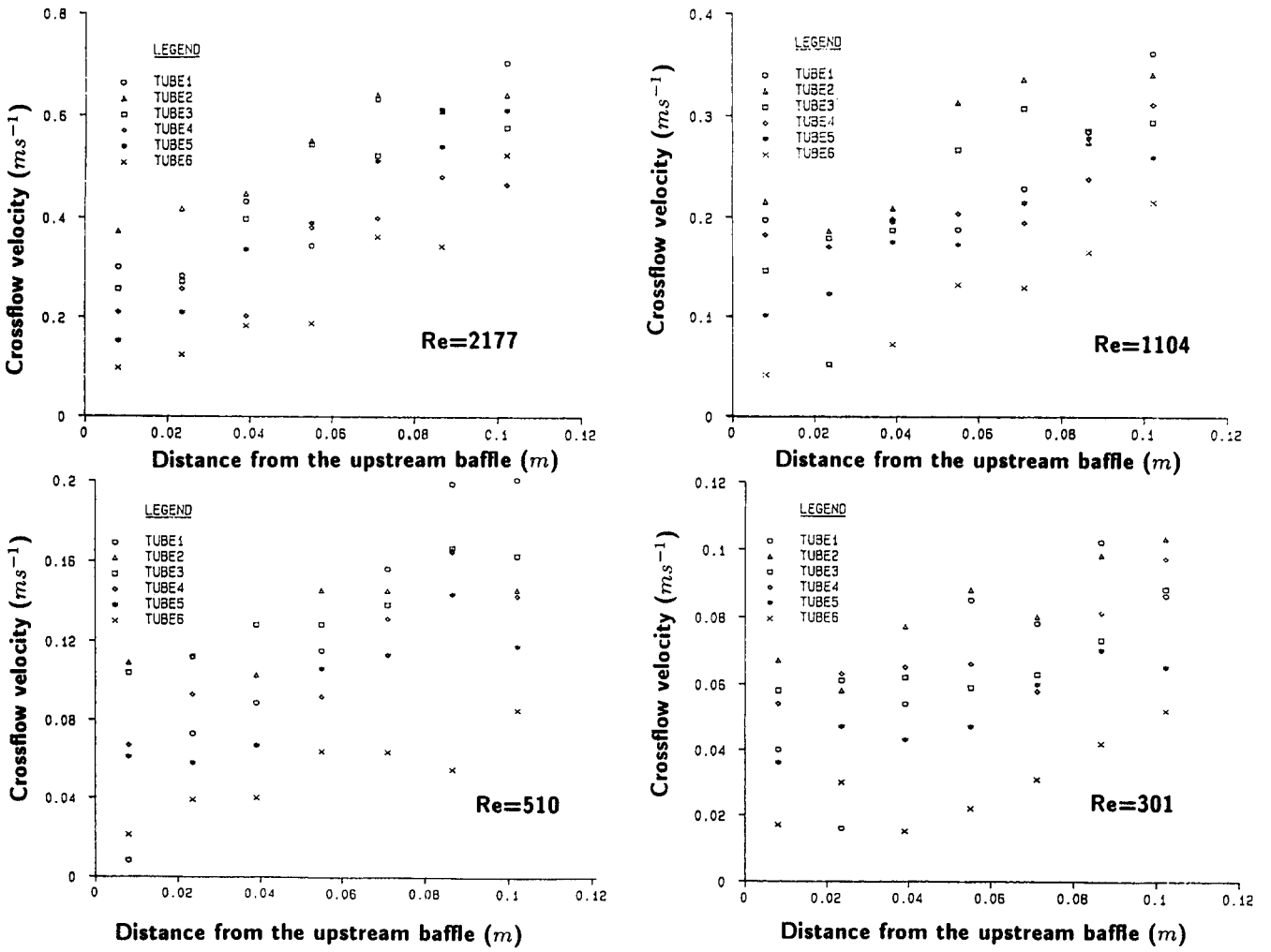

Figure 7 Measured cross-flow velocity variations in a baffle compartment. (a) Re = 2,177; (b) Re = 1,104; (c) Re = 510; (d) Re = 301

the consequent formation of an attached recirculation zone, as found by Murray (1988), Gupta and Katz (1957), and Perez (1984). Depending on the geometry and the Reynolds number, the recirculation zone may reach halfway across the bundle. The effective area available for cross-flow is thus distributed with a bias towards the downstream baffle;

- the axial variation of cross-flow velocity is greater at higher Reynolds numbers.

Radial velocity variations in a baffle space between the central vertical plane of the bundle and shell wall are shown in Figure 8 as cross-flow mass flow rate against the radial distance for the four Reynolds numbers studied. Again two key features appear in this figure.

- The cross-flow velocity decreases with increasing distance between the central vertical plane of the bundle and the shell wall. This may be accounted for by the relatively wide gap between the bundle and shell wall in the horizontal diametral plane of the bundle (see Figure 2);
- the cross-flow velocity distributions, as expected, are more uniform and the variations of the cross-flow along the pass partition lane from the center towards the shell wall are less significant at lower Reynolds numbers.

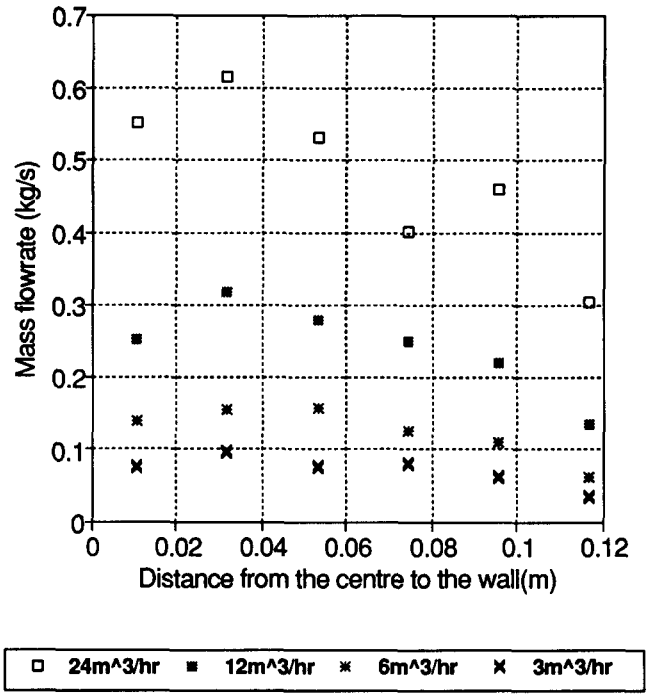

Figure 8 Variations of cross-flow mass flow in a baffle compartment with the radial distance

Cross-flow pressure drop

To be consistent with direct velocity measurements and to facilitate comparison with them, pressure-drop data measured between three pairs of pressure tappings located symmetrically about the pass partition lane in the baffle overlap region are interpreted as cross-flow velocities. Flow velocities were calculated from cross-flow pressure drop using the ESDU (1974, 1979) correlation for pressure loss in tube arrays in which Reynolds number and cross-flow velocity are defined as follows:

$$\mathrm{Re}_c = \frac{M_c D_t}{\mu A_c} \tag{3}$$

$$V_c = \left(2\Delta P_c \frac{D_t}{L}\frac{1}{C\rho\varphi_1\varphi_2}\right)^{1/2} \tag{4}$$

where ΔP_c is the cross-flow pressure drop, D_t is the tube diameter, M_c is the cross-flow mass flowrate, A_c is the cross-flow area of tube-free duct, C is a pressure-drop loss coefficient, φ_1 is a viscosity correction factor, and φ_2 is a roughness correction factor. The above-defined velocity is the superficial velocity in the cross-flow section of a "tube-free" duct, and so in order to obtain cross-flow velocity for the tube bundle geometry studied, superficial velocities were corrected by an area correction factor of 2.085 (the ratio of tube-free duct area calculated from the actual exchanger geometry to the total cross-flow area in the pass partition lane where the cross-flow velocity measurements were made). The ESDU method is based on extensive data, and is considered to be adequate for the task of dealing with the overall magnitude of cross-flow fraction in the tube bundle.

Cross-flow pressure drop in the baffle overlap region was characterized in terms of pressure differences between three pairs of pressure tappings. Referring to Figure 2, these were each symmetrical about the pass partition lane and are hereafter referred to as A (ΔP_{6-9}), B (ΔP_{7-8}), and C (ΔP_{1-2}). It will be noted that tapping pair A gives the pressure difference between the two outer rows of the tubes of the baffle overlap region and on the shell centerline, tapping pair B gives the pressure difference between the penultimate rows of the inlet and outlet sections of the baffle overlap region (on the centerline again), while tapping pair C gives the pressure difference across the same row as B but close to the bypass region adjacent to the shell wall.

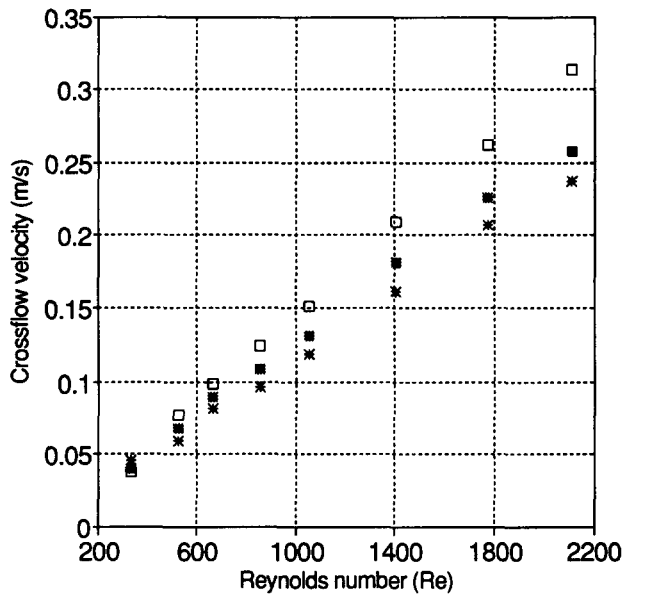

Figure 9 The cross-flow pressure-drop variations (interpreted as cross-flow velocity) with Reynolds number at midway between the baffles ($B_f = 0.50$)

The pressure-drop variations measured in compartment 5 are presented as a function of Reynolds number in Figure 9. These data were obtained midway between the baffles ($B_f = 0.50$) using tapping pairs A, B, and C, respectively. As seen from this figure, the cross-flow pressure drop depends

strongly on Reynolds number. At lower Reynolds numbers, shellside flow is seen to be more uniform. This confirms results of direct cross-flow velocity measurements. The slightly stronger variation of pressure drop at Reynolds numbers below 1300 indicates the existence of a flow transition. This transition was observed at approximately the same Reynolds number by Murray (1988).

The variations of the cross-flow pressure drop with the distance between the baffles showed that the highest cross-flow velocities (i.e., the highest cross-flow pressure drops) occur near the downstream baffle, confirming direct cross-flow velocity measurements. The cross-flow pressure drop variation with distance between the baffles increased with increasing Reynolds number, indicating increasing flow maldistribution with increasing Reynolds number.

The radial variation of cross-flow pressure drop between the central plane of the bundle and the shell wall showed that the cross-flow pressure drop is higher in the central plane than near the shell wall, a fact corroborated by our direct velocity measurements and Murray's pressure-drop measurements (1988).

Comparison between present pressure-drop measurements and the data of Bergelin et al. (1952), obtained by using a rig known as Model 3 in the Delaware University Research Program, is shown in Figure 10. The Delaware data was obtained from an idealized rectangular tube bank configuration, and the shellside flow was therefore free from the flow pattern complications that exist in the baffled cylindrical system used in the present study. However, when we compare our pressure drop data obtained using tapping pair B, which is in the cross-flow region and where the flow cross-sectional area does not vary very rapidly, then there is a similar variation with cross-flow Reynolds number, as shown in Figure 10. In contrast, using our data obtained from tapping pair A, which includes more complex flow regions and flow-area variations, the behavior is quite different, particularly at high flow rates, again shown in Figure 10. It is evident from these comparisons

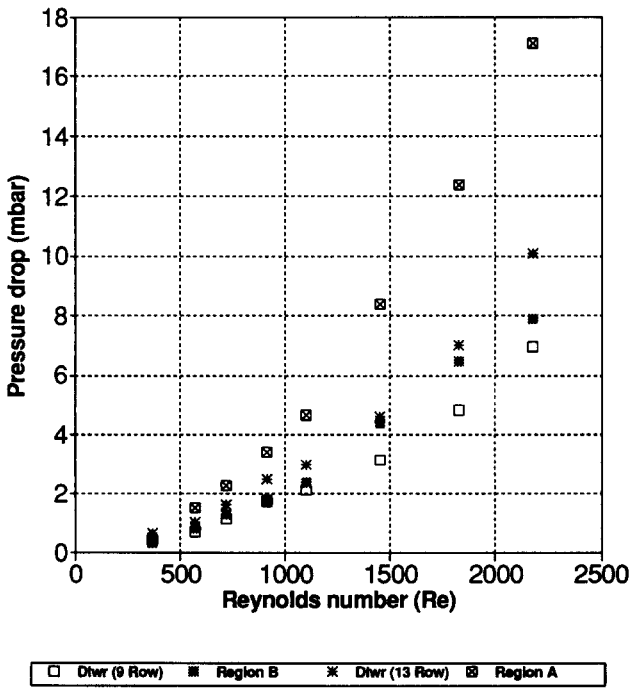

Figure 10 Comparison between present pressure-drop measurements and Delaware University's data

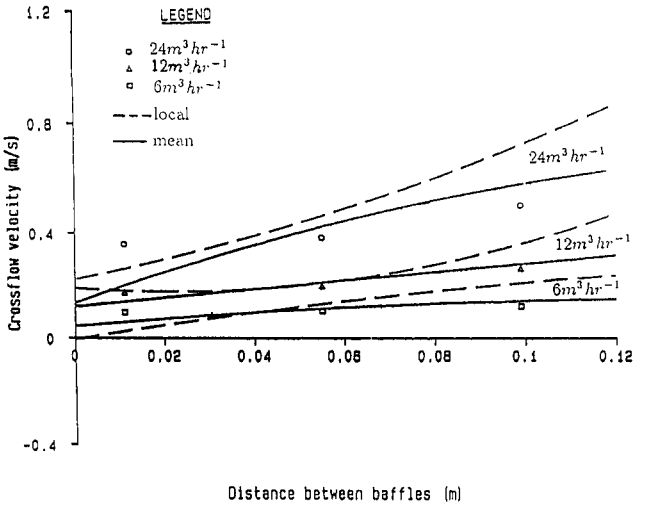

Figure 11 Comparison between the velocities deduced from cross-flow pressure drop measurements and direct cross-flow velocity measurements

that care should be exercised when using flow data obtained on simple tube banks to describe the shellside flow in a baffled shell and tube heat exchanger.

Comparison between pressure-drop measurements and velocity measurements

The pressure differences measured between the two pressure tappings in the central vertical plane of the tube bundle and on the baffle cut line (tapping pair B; see Figure 2) and in the three axial positions, $B_f = 0.10$, 0.50, and 0.90, were taken as samples of the cross-flow pressure-drop distribution. From this pressure data, corresponding bundle flow velocities could be deduced using the ESDU (1974, 1979) correlations for pressure loss in tube arrays.

Figure 11 shows a comparison between the velocities derived from the pressure measurements and the profiles fitted to the velocities measured directly. Data are shown for three flow rates, and two profiles are given in each case. The broken curves were constructed from velocities measured in the pass partition lane but in a tube position that is on the same vertical plane with pressure tapping pair B. The full curves were constructed from averages of velocities measured over all tube positions in the pass partition lane. Agreement between the measured velocities and those derived from pressure-drop measurements is generally reasonable, being better for the profiles based on mean rather than local velocity values. The pressure measurements tend to show rather less variation from upstream to downstream baffle than do the direct velocity measurements.

Conclusions

Shellside cross-flow velocity measurements have been made within the horizontal pass partition lane of an E-type cylindrical shell and tube heat exchanger using a particle tracking technique, and some representative results have been given. The following general features of the cross-flow component within the tube bundle are apparent:

- the cross-flow velocity variation in a baffle space within a shell and tube heat exchanger increases with increasing distance between the upstream and downstream baffles. This axial heterogeneity increases with flow rate;

- the cross-flow velocity decreases with increasing radial distance between the central vertical plane of the bundle and the shell wall. The radial heterogeneity increases with flow rate;
- the highest cross-flow velocities were observed in the center of the bundle adjacent to the downstream baffle, while very low velocities were observed near the upstream baffle and near the shell wall. These low velocities suggest that the recirculation zone just downstream of the upstream baffle edge is more extensive near the shell wall than in the center of the bundle.

Pressure-drop measurements were made in the shellside flow of the same heat exchanger using pressure tapped instrument tubes. The conclusions drawn from these measurements are as follows:

- the cross-flow pressure drop is a strong function of Reynolds number. At lower Reynolds number, the cross-flow pressure distribution within a compartment space is more uniform;
- the variation of cross-flow pressure drop with distance between the baffles increases with increasing Reynolds number, indicating increasing flow nonuniformity, in an axial direction, with increasing Reynolds number;
- the cross-flow pressure drop is higher at the central plane of the bundle than the shell wall. The radial pressure drop variations decrease with increasing distance between the upstream and downstream baffles;
- independently measured cross-flow velocities were shown to be consistent with the velocities derived from the cross-flow pressure-drop measurements.

References

Bell, K. J. 1980. Delaware method for shellside design. In *Heat Exchanger Thermal Hydraulic Fundamentals and Design*. Hemisphere, NATO Adv. Study Institute, Istanbul, Turkey, 537–558

Bergelin, O. P., Brown, G. A. and Doberstein, S. C. 1952. Heat transfer and fluid friction during flow across banks of tubes—IV. A study of the transition zone between viscous and turbulent flow. *Trans. ASME*, **74**, 953–960

Berner, C., Durst, F. and McEligat, D. M. 1984. Flow around baffles. *J. Heat Transfer*, **106**, 743–749

Brown, G. A. 1956. Heat transfer and fluid friction during turbulent flow through a baffled shell and tube heat exchanger. PhD thesis, Dept. of Chemical Engineering, University of Delaware

Diaper, A. D. and Haseler, L. E. 1990a. Bypass flow in the crossflow region of a shell and tube heat exchanger using neutral density particles. *Proc. 9th Int. Heat Transfer Conf. Jerusalem*, 127–132

Diaper, A. D. and Haseler, L. E. 1990b. Crossflow pressure drop and flow distribution of a tube bundle using computational fluid dynamics. *Proc. 9th Int. Heat Transfer Conf. Jerusalem*, 235–240

Engineering Sciences Data Unit (ESDU). 1979. Crossflow pressure loss over banks of plain tubes in square and triangular arrays including the effects of flow direction. Item No 79034, ESDU, UK

Engineering Sciences Data Unit (ESDU). 1974. Pressure loss during crossflow of fluid with heat transfer over a plain tube bank without baffles. Item No 74040, ESDU, UK

Gupta, R. K. and Katz, D. L. 1957. Flow pattern for predicting shellside heat transfer coefficients for baffled shell and tube heat exchangers. *Indust. Eng. Chem.*, **49** (6), 998–999

Johnston, D. and Wills, M. J. 1984. The predictions of shellside flow distribution and pressure drop in shell and tube heat exchangers. *1st UK Natl. Heat Transfer Conf., Leeds*, **2**, 1163–1167

Keene, L. W., Gibbons, D. B. and Davies, T. W. 1991. Shellside pressure drop with no tubes in the window and sealing strips. *HTFS Symp.*, Canterbury, UK

Leighton, M. D. 1955. Pressure drop in a baffled tubular exchanger without internal leakage. M.Ch.E. thesis, Dept. of Chemical Engineering, University of Delaware

Murray, P. W. 1988. Flow and pressure drop on the shellside of cylindrical shell and tube heat exchangers. Ph.D. thesis, Dept. of Chemical Engineering, University of Aston in Birmingham, UK

Palen, J. W. and Taborek, J. 1969. Solution of shellside flow pressure drop and heat transfer by stream analysis method. *10th Natl. Heat Transfer Conf., AIChE–ASME*, 53–65

Pekdemir, T. 1990. Flow pattern and pressure drop on the shell side of a cylindrical shell and tube heat exchanger. M.Phil. thesis, Dept. of Chemical Engineering, University of Exeter, Exeter, UK

Perez, J. A. 1984. Internal heat transfer and pressure drop measurements in a variously shell and tube heat exchangers. Ph.D. thesis, Dept. of Mechanical Engineering, University of Minnesota

Tinker, T. 1947. Shellside heat transfer characteristics of segmentally baffled shell and tube heat exchangers. *ASME Annu. Meeting*, 293–304

Zukauskas, A. and Winskas, R. 1983. Banks of plain and finned tubes. *Heat Exchanger Design Handbook* (*HEDH*). Hemisphere, Sec. 2.2.4